Uher G, Pillans JJ, Hatton AD, Upstill-Goddard RC. Photochemical oxidation of dimethylsulphide to dimethylsulphoxide in estuarine and coastal waters. *Chemosphere* 2017, 186, 805-816.

Chemosphere 186 (2017) 805–816

Contents lists available at ScienceDirect

Chemosphere

journal homepage: www.elsevier.com/locate/chemosphere

Photochemical oxidation of dimethylsulphide to dimethylsulphoxide in estuarine and coastal waters

Günther Uher [a, *], J. Julian Pillans [a, 1], Angela D. Hatton [b, 2], Robert C. Upstill-Goddard [a]

[a] School of Natural and Environmental Sciences, Newcastle University, Newcastle upon Tyne, NE1 7RU, United Kingdom
[b] Scottish Association for Marine Science, Dunstaffnage Marine Laboratory, Oban, Argyll, PA37 1QA, United Kingdom

HIGHLIGHTS

- We observed 1:1 M conversion of DMS to DMSO in estuarine waters.
- This suggests that DMS photo-oxidation occurred via the CDOM sensitised $^1O_2$ pathway.
- Photochemical rate constants decreased ~10-fold from river to seawater.
- Rate constants were strongly correlated with CDOM absorption coefficients (a_{350}).
- a_{350}-normalised rate constants increased ~10-fold from river to seawater.

ARTICLE INFO

Article history:
Received 30 November 2016
Received in revised form
9 August 2017
Accepted 10 August 2017
Available online 11 August 2017

Handling Editor: Jun Huang

Keywords:
Reduced sulfur compounds
Coloured dissolved organic matter
Tyne estuary
North Sea
Seawater
Photochemistry

ABSTRACT

Dimethylsulphide (DMS) photo-oxidation and dimethylsulphoxide (DMSO) photoproduction were estimated in 26 laboratory irradiations of coastal samples from NE England (Tyne estuary) and W Scotland (Loch Linnhe and River Nant at Taynuilt). Pseudo-first order rate constants of DMS photo-oxidation (0.038 h^{-1} to 0.345 h^{-1}) and DMSO photo-production (0.017 h^{-1} to 0.283 h^{-1}) varied by one order of magnitude and were lowest in the coastal North Sea. Estuarine samples (salinity $S < 30$) had a mean DMSO yield of 96 ± 16% ($n = 14$), consistent with 1:1 M conversion via photosensitised oxidation by singlet oxygen. Photochemical rate constants were strongly correlated with coloured dissolved organic matter (CDOM) absorption coefficients at 350 nm, a_{350}. Variations in a_{350} explained 61% ($R^2 = 0.61$, $n = 26$) and 73% ($R^2 = 0.73$, $n = 17$) of the variability in DMS photo-oxidation and DMSO production, respectively. However, CDOM normalised photochemical rate constants increased strongly towards coastal waters exhibiting lowest CDOM absorbance, indicating water samples of marine character ($S > 30$) to be most reactive with respect to DMS photo-oxidation. Estimates of water column averaged DMS photo-oxidation rate constants, obtained by scaling to mean daily irradiance (July, NE England) and mid-UV underwater irradiance, were 0.012 d^{-1}, 0.019 d^{-1}, and 0.017 d^{-1} for upper estuary ($S < 20$), lower estuary ($20 < S < 30$) and coastal waters ($S > 30$), at the lower end of previous observations. Comparing our water column averaged DMS photo-oxidation rate constants with estimated DMS losses via air-sea gas exchange and previously reported biological consumption implies that DMS photochemical removal is of only minor importance in our study area.

1. Introduction

Dimethylsulphide (DMS) is an important biogenic trace gas implicated in the regulation of global climate. Marine DMS emissions may account for ~20–35 Tg (S) a^{-1} globally (Simo and Dachs, 2002; Kloster et al., 2006; Lana et al., 2011; Land et al., 2014) and likely dominate the southern hemisphere tropospheric sulphur budget (12 Tg (S) a^{-1}; Stern, 2006; Lana et al., 2012; Land et al., 2014). A marine DMS-climate feedback loop was first proposed

* Corresponding author.
E-mail address: guenther.uher@ncl.ac.uk (G. Uher).
[1] Now at Estuarine and Coastal Monitoring and Assessment Service, Environment Agency, Manley House, Kestrel Way, Exeter, EX2 7LQ, United Kingdom.
[2] Now at National Oceanography Centre, University of Southampton Waterfront Campus, European Way, Southampton, SO14 3ZH, United Kingdom.

http://dx.doi.org/10.1016/j.chemosphere.2017.08.050

by Charlson et al. (1987), in which gas to particle conversion of phytoplankton-derived DMS in the marine boundary layer produces sulphate aerosols that act as cloud condensation nuclei, thereby impacting Earth's radiation balance via changes to cloud albedo. While some recent modelling studies imply a rather weak marine DMS-climate feedback (Carslaw et al., 2010; Quinn and Bates, 2011), others support the notion that cloud condensation nuclei abundance may be controlled by DMS-derived and other secondary aerosols (Lana et al., 2012). Considerable uncertainty regarding the contribution of DMS to indirect aerosol forcing (Carslaw et al., 2013; Woodhouse et al., 2013) illustrates the need for further studies of biogeochemical DMS cycling.

Marine DMS is primarily derived from the enzymatic breakdown of dimethylsulphonio-propionate (DMSP), an algal osmolyte and cryoprotectant (Simó, 2001). Sea surface DMS losses are usually dominated by microbial consumption or photodegradation, with only minor contributions from air-sea exchange (Archer et al., 2002; Toole et al., 2006; Vila-Costa et al., 2008; Galí and Simó, 2015). Results from ^{35}S-DMS tracer experiments indicate that microbial DMS consumption in surface waters primarily yields dimethylsulphoxide (DMSO) (Del Valle et al., 2007b). By contrast, the DMSO yield from DMS photo-oxidation apparently varies between shelf seas (25%), polar waters (39%) and the open ocean (14%) (Kieber et al., 1996; Hatton, 2002; Toole et al., 2004). Even so, DMSO concentrations frequently exceed those of DMS (Lee et al., 1999), possibly due to a lack of photochemical removal (Toole et al., 2004), slow microbial consumption (Tyssebotn et al., 2017), significant biological production (Del Valle et al., 2007a) or an aggregate of all three.

Laboratory studies established that aqueous solutions of dialkylsulphides undergo photosensitised oxidation to their respective sulphoxides (e.g. Sysak et al., 1977), involving singlet oxygen ($^1O_2$) formation via chromophoric photosensitisers, and 1:1 M conversion to the sulphoxide. Brimblecombe and Shooter (1986) showed that marine chromophoric dissolved organic matter (CDOM) sensitises DMS photo-oxidation, consistent with singlet oxygen ($^1O_2$) formation via electronically excited triplet states in natural CDOM (Zepp et al., 1985). However, Brimblecombe and Shooter (1986) did not report DMSO concentrations, and subsequent work reported low DMSO yields, particularly in open ocean waters (Kieber et al., 1996; Hatton, 2002; Toole et al., 2004), that are not consistent with the $^1O_2$ pathway. Positive correlations of DMS photo-oxidation rates with nitrate concentrations imply that reactive intermediates deriving from nitrate photolysis are also involved in DMS photodegradation (Bouillon and Miller, 2004; Toole et al., 2004). Their likely contribution, as estimated from relationships between photo-oxidation rate constants and in-situ nitrate concentrations, appears to be rather variable between contrasting open ocean waters of the subpolar South Pacific (35%; Toole et al., 2004) and NE Pacific (81%; Bouillon and Miller, 2004). By implication, these results suggest highly variable contributions from CDOM related pathways of DMS photo-oxidation (19–65%). Data on the relationship between DMS photo-oxidation rate constants and nitrate concentrations remain scant. However, a recent meta-analysis of both available and unpublished apparent quantum yields of DMS photo-oxidation suggested that photochemical DMS removal is primarily controlled by CDOM nature and abundance, while the overall contribution of nitrate related pathways is likely limited to ~20–25% (Galí et al., 2016). Concurrent studies of the effects of CDOM and nitrate on DMS photo-oxidation are needed to further constrain the roles of contrasting photodegradation pathways at regional scales.

Due to their characteristically high DMS concentrations, coastal waters are thought to be disproportionately large contributors to global marine DMS emissions (Uher, 2006). UV light absorption by CDOM, a proxy for the photosensitisation capacity of natural waters (Zepp et al., 1985) is also high in coastal waters (Stedmon and Nelson, 2014). Given the high levels of natural photosensitisers, it is plausible to assume that CDOM related DMS photo-degradation, including CDOM sensitised photo-oxidation by $^1O_2$, is important in controlling coastal DMS concentrations and sea-to-air flux. In this paper we evaluate the results of irradiation experiments using estuarine and coastal waters collected along the UK northeast and northwest coasts. DMS photo-degradation and DMSO photo-production were quantified, with the DMSO yield used to diagnose photosensitised DMS oxidation by $^1O_2$. Rate constants for DMS photo-oxidation and concurrent DMSO production were compared to spectral CDOM absorbance in the UV and visible domains to test for predictive relationships between photochemical DMS removal and proxies of the photo-sensitisation capacity of natural waters.

2. Methods

2.1. Study areas and sampling

A total of 16 surface water samples were collected from the Tyne estuary, NE England, and adjacent North Sea waters, and a further 2 samples were obtained from Loch Linnhe and the River Nant at Taynuilt, W Scotland (Table 1, Fig. 1). Both study areas receive river discharge rich in dissolved organic carbon (DOC) due to extensive blanket peat coverage in their catchments (Hope et al., 1997; Joint Nature Conservation Committee, 2011). The Tyne estuary is a ria type, macrotidal estuary of 33 km length, receiving a mean freshwater discharge of ~45 $m^3 s^{-1}$ from the River Tyne (Manning, 2012). Loch Linnhe is a large Scottish sea loch of fjordic character, extending approximately 60 km in length from its north-eastern end to the coastal waters of the Inner Hebrides to the southwest. Loch Linnhe is connected with Loch Eil and, via River Lochy, with Loch Lochy to the north, receiving significant runoff (112.5 $m^3 s^{-1}$), dominated by River Lochy discharge (59.5 $m^3 s^{-1}$) to its northern end (Manning, 2012). The Lochy and Tyne rank among the 10 largest UK rivers by discharge (National River Flow Archive, http://nrfa.ceh.ac.uk/). The River Nant is a small Scottish river of ~10 km length discharging freshwater from Loch Nant into Loch Etive, which connects with Loch Linnhe at Connel, Argyll and Bute, Scotland.

Surface water samples for subsequent irradiation experiments were collected in 25 L high density polyethylene (HDPE) carboys pre-cleaned with laboratory detergent, (Decon 90), 10% HCl, and "Milli-Q" analytical grade laboratory water (Millipore Q185, 18.2 Ohm Milli-Q, Millipore System Inc., USA). Tyne estuary and adjacent North Sea samples were immediately transferred to our Newcastle laboratory and pressure filtered (Gelman, No. 15207, stainless steel, <0.7 bar N_2) with sequential inline filtration (Pall Corp.: 0.7 μm, 142 mm diameter TCLP glass fibre filter; Sartorius, 0.2 μm Sartopore 2 Gamma capsule filter). Loch Linnhe and River Nant samples were filtered by tangential flow (Millipore, Pellicon, 0.2 μm cassette filter) at Dunstaffnage Marine Laboratory in Oban. All filtration was completed on the day of sampling, usually within 4 h of collection. Samples were dark stored at 5 °C in HDPE carboys, prior to their irradiation during the following 16 days (Table 1). Loch Linnhe and River Nant samples were transferred to Newcastle for irradiation.

2.2. Irradiation experiments

DMS concentrations often decreased to <0.2 nM for river waters and <1 nM for sea waters during storage. Therefore, prior to irradiation (in Newcastle) and immediately following their re-filtration

Table 1
Summary of irradiation experiments in the Newcastle solar simulator, including sampling locations, collection date, and storage time until irradiation, +Irr. Sample salinities, CDOM absorption coefficients, a_{350}, and spectral slope factors, $S_{290\text{-}350}$, at the start of the irradiations are also listed. DMS_i denotes the initial DMS concentration at the start of the experiments. Pseudo first order rate constants of DMS photo-oxidation, k_{DMS}, and DMSO photoproduction, k_{DMSO}, and their standard errors are corrected for self-shading (see Methods for details). * Note that k_{DMS} for experiment 14 represents the arithmetic mean and standard deviation of 5 individual irradiations with DMS_i ranging from 6.1 to 41.1 nM.

No	Location	Latitude	Longitude	Date Collected	+Irr	Salinity/-	a_{350}/m^{-1}	$S_{290\text{-}350}/nm^{-1}$	DMS_i/nM	DMS photolysis k_{DMS}/h^{-1}	DMSO Production k_{DMSO}/h^{-1}	Molar conversion %
Tyne Estuary												
1	Wylam	54.9755	−1.8152	10/07/2003	+6	0.1	30.9	0.0141	3.5	0.183 ± 0.030	N/A	N/A
2				21/08/2003	+1	0.1	20.1	0.0147	4.3	0.134 ± 0.014	N/A	N/A
3				21/08/2003	+7	0.1	20.2	0.0143	9.3	0.107 ± 0.004	N/A	N/A
4				15/12/2003	+2	0.1	46.8	0.0134	10.9	0.199 ± 0.014	0.197 ± 0.010	93
5				19/01/2004	+2	0.2	38.8	0.0135	4.1	0.187 ± 0.014	0.218 ± 0.013	113
6				19/01/2004	+16	0.2	39.2	0.0135	8.2	0.133 ± 0.019	0.236 ± 0.013	120
7				09/03/2004	+2	0.2	26.9	0.0138	5.6	0.220 ± 0.002	0.167 ± 0.005	87
8				21/03/2004	+4	0.1	47.4	0.0138	8.0	0.181 ± 0.018	0.136 ± 0.024	94
9				19/04/2004	+2	0.1	18.3	0.0150	7.2	0.194 ± 0.007	0.128 ± 0.021	104
10				19/04/2004	+3	0.1	18.0	0.0150	7.3	0.194 ± 0.007	0.113 ± 0.016	88
11				19/05/2004	+5	0.1	19.6	0.0151	7.8	0.187 ± 0.016	0.185 ± 0.011	88
12				25/06/2004	+1	0.1	18.6	0.0153	10.0	0.125 ± 0.005	0.089 ± 0.005	74
13				25/06/2004	+4	0.1	71.9	0.0132	8.0	0.323 ± 0.042	0.283 ± 0.040	82
14	*			25/06/2004	+12	0.1	71.5	0.0133	6.1–41.1	0.345 ± 0.016	N/A	N/A
15				20/07/2004	+1	0.2	16.8	0.0151	6.4	0.186 ± 0.028	N/A	N/A
16				20/07/2004	+3	0.2	16.8	0.0151	8.2	0.218 ± 0.021	N/A	N/A
17				20/07/2004	+7	0.2	16.7	0.0151	10.2	0.211 ± 0.008	N/A	N/A
18				20/07/2004	+13	0.2	16.6	0.0151	10.5	0.220 ± 0.022	N/A	N/A
19	Newcastle	54.9676	−1.6077	09/03/2004	+2	5.0	22.0	0.0141	5.6	0.259 ± 0.010	0.115 ± 0.010	88
20	N. Shields	55.0068	−1.4377	19/01/2004	+3	23.3	4.2	0.0137	7.3	0.091 ± 0.003	0.130 ± 0.004	105
21				09/03/2004	+2	23.6	5.1	0.0149	5.4	0.074 ± 0.003	0.078 ± 0.003	129
North Sea												
22	Cullercoats	55.0349	−1.4306	09/03/2004	+2	31.3	1.3	0.0149	5.3	0.039 ± 0.000	0.017 ± 0.001	52
23				20/07/2004	+1	32.0	1.4	0.0142	7.3	0.038 ± 0.003	N/A	N/A
24	North Sea	55.1166	−1.3333	30/03/2004	+2	34.5	1.1	0.0130	7.8	0.052 ± 0.002	0.038 ± 0.001	74
Scottish West Coast												
25	River Nant at Taynuilt	56.4333	−5.2374	05/05/2004	+7	0.1	21.6	0.0141	14.3	0.159 ± 0.023	0.094 ± 0.008	78
26	Loch Linnhe	56.5407	−5.4331	05/05/2004	+6	31.9	1.7	0.0150	8.3	0.044 ± 0.006	0.037 ± 0.008	55

(0.2 μm Sartopore 2 Gamma capsule filter) to minimise microbial activity, samples were transferred to a series of 2 L HDPE carboys and augmented with a DMS stock solution, to adjust their initial DMS concentrations to within the range typical of European estuarine and coastal waters. Our average initial DMS concentration was 7.6 nM, comparable to the mean European shelf water concentration during summer (8.4 nM; Uher, 2006). The DMS stock was prepared by injecting pure DMS (Sigma-Aldrich, 99+%, No. 27,438-0) into a Milli-Q-filled, 50 ml crimp top vial. The sealed solution was homogenised using a magnetic stirrer and used to create a working stock solution by further dilution into a second crimp top vial. After adding the appropriate volumes of working stock the sample carboys were filled with further sample to exclude all headspace and homogenised with a magnetic stirrer. The DMS-augmented samples were then dispensed via short lengths of silicone tubing into a series of headspace free, gas tight cylindrical quartz irradiation flasks (50 ml), closed off with compression fittings (Swagelok, ¼″ Nylon end caps, No. NY-400-C). For irradiation, flasks were mounted vertically in a solar simulator carousel surrounding an ozone free 300 W Xe-arc lamp mounted inside a borosilicate sleeve to remove UVC irradiance; lamp spectral output is broadly similar to midsummer, noon clear sky irradiance in Newcastle (Kitidis et al., 2008). The solar simulator was air-cooled (two 19W cooling fans) to keep samples at laboratory temperature (20±2 °C). We did not determine the spectral output of our light source immediately prior to our study but we did subsequently determine its broadband UV (300–400 nm) and visible (400–800 nm) irradiances with a spectroradiometer (ILT950, International Light Technologies); these were 35.4 W m^{-2} and 277 W m^{-2} respectively. Irradiations ran for periods of 6–30 h, during which times a minimum of 3 subsamples were removed for analysis. We also ran dark controls wrapped in tin foil to exclude light but otherwise treated identically to their irradiated counterparts.

For selected samples, simultaneous sunlight and laboratory irradiations facilitated a direct comparison of solar simulator irradiance with irradiance under ambient conditions. Sunlight irradiations were on the roof of the Newcastle laboratory during July and August 2004, between 10:00 and 15:00 local time. Quartz irradiation flasks were laid horizontally in plastic trays continuously flushed with tap water to maintain the temperature close to that of ambient North Sea water (11±1 °C).

2.3. DMS and DMSO analysis

Dissolved DMS was determined by helium purging, followed by gas chromatography (Shimadzu, GC14B) and sulphur chemiluminescence detection (Sievers, 350B), using a method modified from Uher and Andreae (1997). Water samples were transferred from the irradiation flasks into ground glass syringes, with known volumes (up to 40 ml) then injected into a series of 120 ml purging vessels via side ports fitted with gas tight stopcocks. Each sample was helium-purged for 14 min at 85 ml min^{-1}. The helium stream (BOC N4.6) passed through a U-shaped borosilicate water trap (35 cm × 10 mm i.d.; −20 °C) and into a liquid nitrogen cryotrap (perfluoroalkoxy (PFA) tubing, 75 cm × 1.65 mm, packed with

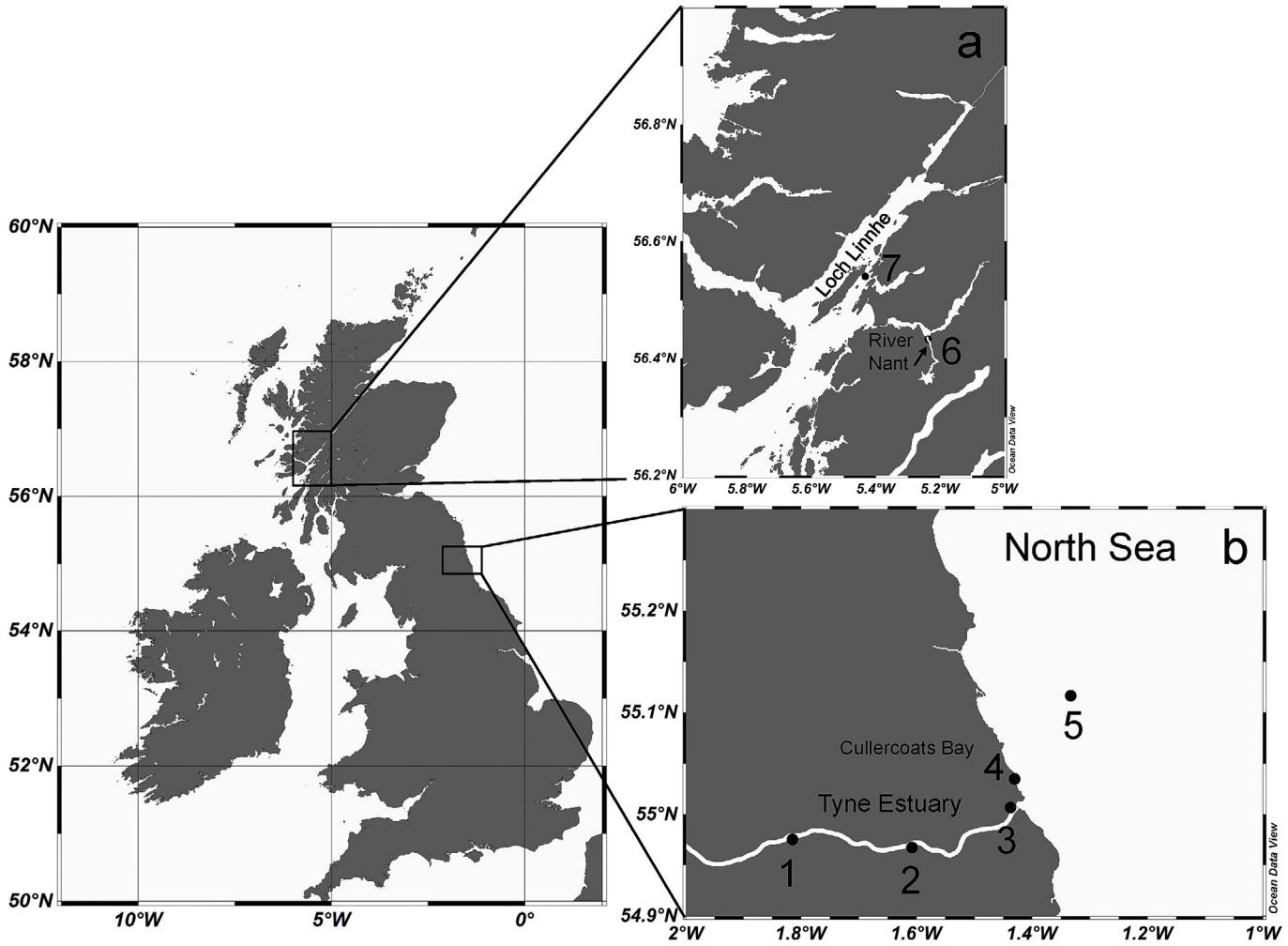

Fig. 1. Sampling locations in W Scotland (a) and the Tyne estuary and adjacent North Sea (b). Tyne Estuary: Wylam (1), Newcastle (2), North Shields (3), Cullercoats Bay, and coastal North Sea (5). W Scotland: River Nant at Tanuilt (6) and Loch Linnhe (7). See Table 1 for further details. Study area maps were created with Ocean Data View, Schlitzer, R., http://odv.awi.de, 2014.

20 mm silanised glass wool) attached to a 4-port injector valve (Vici Valco 4UWE). Once purging was completed, a second helium stream (30 ml min^{-1}) transferred the cryotrapped sample to a liquid nitrogen cryofocussing loop (PFA, 25 cm × 0.8 mm, packed with 10 mm silanised glass wool) connected to the gas chromatograph's 6-port injection valve (Vici Valco, C6UWE). After 5 min the 6-port valve was actuated with the cryoloop submerged in warm water, thereby injecting the cryo-concentrated sample onto the GC column (Chrompak Porabond Q, 25 m × 0.32 mm; helium carrier gas, 5 ml min^{-1}). DMS was baseline separated from other sulphur gases by a two-stage temperature programme (1.2 min at 60 °C, 40 °C min^{-1}, 1 min at 180 °C), and eluted at a retention time of 3.8 min. Two stripping channels were used simultaneously to increase sample throughput. All glassware was silanised (Sigma-Aldrich, Sylon CT, No. 33065-U), and all connections used PFA tubing (Fluoroware) with Nylon compression fittings (Swagelok) to minimise DMS adsorption onto internal system surfaces.

DMSO was analysed after enzymatic reduction to DMS Hatton et al. (1994). Following DMS purging and analysis, 3 ml of an aqueous solution containing 30 mM EDTA, 540 μM flavin mononucleotide, and 18.5 μg ml^{-1} DMSO reductase was added to each of the purging vessels. To facilitate enzymatic reduction, these were next each illuminated by three incandescent 60 W light bulbs and purged for 18 min to enable complete DMSO conversion to DMS, with the purged DMS analysed as described above.

Method calibration was with DMS emitted from a gravimetrically calibrated permeation device (Vici Metronics, Type 6200, 51 ± 1 ng DMS min^{-1}) maintained in a temperature controlled chamber (30 °C) flushed with synthetic air (30 ml min^{-1}). Gravimetrically calibrated sample loops were used to inject varying volumes of permeation gas onto the cryofocusing loop. Calibrations using gaseous standards and aqueous standards prepared by diluting stock DMSO (99.9%, Sigma-Aldrich, No. 27,043-1) agreed to within ±1% and were linear over the range 1–50 ng DMS (R^2 = 0.996, n = 13). This corresponds to DMS concentrations of 0.8–80 nM using 20 ml and 40 ml sample volumes respectively. The overall precision of the method was better than ±5% based on replicate injections of gaseous DMS standards. Considering cumulative errors in sample loop volumes, DMS mass losses from the permeation device and air flow through the permeation chamber (<±5%), we estimate the overall analytical error of the method at better than ±10%.

2.4. CDOM absorbance spectra and ancillary data

CDOM absorbance in the UV and visible range (250–800 nm)

was recorded on a double beam spectrophotometer (Kontron, Uvikon 923), using quartz cells with optical path lengths of 10 mm or 100 mm. Milli-Q was used as a reference. Spectra were corrected for refractive index effects and instrument drift by subtracting the mean absorbance over the wavelength range 680–700 nm (Kitidis et al., 2008). Absorption coefficients were calculated from

$$a_\lambda = \ln(10)\, A_\lambda\, d^{-1} \quad (1)$$

where a_λ is the Napierian absorption coefficient (m^{-1}) at wavelength λ, Aλ is the absorption at wavelength λ, and d is the optical path length (m). We adopted the absorption coefficient at 350 nm (a_{350}) as a proxy for CDOM, because a_{350} is a robust predictor of DOC levels in our study area (Spencer et al., 2007a) and is representative of photochemically active chromophores in the mid-UV range (Kitidis et al., 2008). The spectral slope factor over the wavelength range 290–350 nm ($S_{290\text{-}350}$) was estimated from a non-linear fit to a single exponential model

$$a_\lambda = a_{\lambda 0} \exp(-S_{290\text{-}350}\,(\lambda - \lambda_0)) \quad (2)$$

where $a_{\lambda 0}$ is the absorption coefficient at the reference wavelength λ_0 (250 nm). $S_{290\text{-}350}$ was previously shown to discriminate between terrestrial and marine-derived CDOM (Uher et al., 2001; Spencer et al., 2007b), and to indicate CDOM photobleaching, as lowest $S_{290\text{-}350}$ values are associated with newly formed CDOM (Kitidis et al., 2006), while progressive photodegradation increases $S_{290\text{-}350}$ (Kitidis et al., 2008). Salinity was determined using a portable conductivity meter (Hanna, model 8633).

2.5. Calculation of rate constants and molar conversion

Pseudo first order rate constants, k_{DMS}, were derived by regressions to the log-linearised first order rate law,

$$\ln(C_t(DMS)/C_0(DMS)) = -k_{DMS} \times t \quad (3a)$$

where C_t and C_0 are DMS concentrations at time t and t = 0, respectively. To correct for any changes in the DMS concentrations of dark controls, the first order rate constants derived from regressions to DMS concentrations in dark controls were subtracted from those obtained by regressions to irradiated sample concentrations. Pseudo first order DMSO photoproduction rate constants, k_{DMSO}, were obtained in a similar way, except that the DMS concentration at time t, C_t(DMS), was calculated by subtracting the net increase in DMSO concentration between t and t = 0, ΔC_t(DMSO), from the initial DMS concentration,

$$\ln((C_0(DMS) - \Delta C_t(DMSO))/C_0(DMS)) = -k_{DMSO} \times t \quad (3b)$$

Rate constants were divided by the self-shading factor, *f*, to correct for self-shading via intrinsic light absorbance by CDOM. The self-shading factor, *f*, was calculated from

$$f = (1 - \exp(-a_{350}\, d))/(a_{350}\, d) \quad (4)$$

where a_{350} is the CDOM absorption coefficient at 350 nm and d = 0.021 m is the mean optical path length through the quartz irradiation flasks (Kitidis et al., 2008). Below salinity S = 10, *f* varied between 0.5 and 0.84, while for S > 10 samples were optically thin ($f \geq 0.95$). Irradiations of Tyne river water with and without broadband filters (DuPont, Mylar D, 320 nm cut-off) confirmed that UV-A irradiance (≥320 nm) accounted for >65% of total DMS photo-oxidation (data not shown), justifying the use of mid UV CDOM absorption coefficients to calculate *f*.

The overall molar conversion of DMS to DMSO was determined as the average percentage conversion, corrected for changes in dark controls, over the full duration of each irradiation.

3. Results and discussion

3.1. Photodegradation kinetics and DMSO yield

DMS concentrations decreased in all irradiations, accompanied by increases in DMSO (Fig. 2). In dark controls DMS and DMSO showed little to no change, remaining within ±1 nM of their initial concentrations throughout the experiments (<30 h). DMS photo-oxidation and DMSO photoproduction both followed first order kinetics (Fig. 2), in line with previous findings for DMS (Kieber et al., 1996; Brugger et al., 1998; Hatton, 2002; Toole et al., 2004).

Our experimental protocol demanded DMS additions prior to the start of the irradiations, with initial DMS concentrations typically varying from 3.5 nM to 14.3 nM (Table 1). We therefore irradiated a series of Tyne River waters to evaluate any dependence of our pseudo first order rate constants on DMS concentration over the relevant range (6.1–41.1 nM, Table 1, Fig. 3). Initial DMS loss rates, calculated from the product of the initial DMS concentration and the photo-oxidation rate constant, increased linearly with DMS concentration ($R^2 = 0.995$, n = 5; Fig. 3), supporting our assumption of pseudo first order kinetics and consistent with previous conclusions for DMS concentrations <50 nM (Kieber et al., 1996; Brugger et al., 1998).

Table 1 summarises the DMSO yields from DMS photo-oxidation. For estuarine samples (S < 30) the mean DMSO yield was 96 ± 16% (n = 14), consistent with 1:1 M conversion. In 3 experiments (Table 1, No's 5, 6, 21), DMSO yields exceeded the mean by more than one standard deviation. Elevated DMSO yields might suggest the presence of additional DMSO sources other than DMS. However, so far the only known alternative DMSO source is biological production by particle associated processes (Del Valle et al., 2007a) which should have been excluded by our filtration protocols. Another possibility, bacterial reduction of dimethylsulphone (Bentley and Chasteen, 2004), also seems unlikely because dimethylsulphone has not been detected in seawater (Lee et al., 1999). We therefore conclude that elevated DMSO yields likely resulted from combined analytical error across four sample subsets (DMS and DMSO determinations in dark controls and irradiated samples). For samples of salinity >30 the yield was much lower (60 ± 12%, n = 3). The lowest molar conversion percentages were for samples from Cullercoats Bay (52%) and Loch Linnhe (55%), possibly a result of differing sample compositions for estuarine (S < 30) and coastal (S > 30) waters.

The mean (±standard error) of all DMS photo-oxidation rate constants was 0.166 ± 0.016 h^{-1} (n = 26, Table 1). For our sample subset with concurrent DMSO photoproduction data the mean DMS photo-oxidation rate constant (0.157 ± 0.019 h^{-1}; n = 17) agreed closely with the mean DMSO photoproduction rate constant (0.133 ± 0.018 h^{-1}; n = 17). Overall, the rate constants for DMS photo-oxidation and DMSO photoproduction were not significantly different (*t*-test, p = 0.10). These results support a 1:1 M conversion for the majority of samples, particularly for estuarine samples (S < 30) for which allochthonous CDOM is predominantly terrestrially-derived (Uher et al., 2001).

Our finding of 1:1 M conversion of DMS to DMSO is consistent with photo-oxidation by $^1O_2$ deriving from natural photosensitisers in the CDOM pool (Sysak et al., 1977; Zepp et al., 1985; Brimblecombe and Shooter, 1986). DMSO yields close to 100% for estuarine waters (S < 30) imply photosensitised oxidation by $^1O_2$ to be the dominant DMS photodegradation pathway. Although DMSO yields for our coastal samples (S > 30) were lower (52–78%,

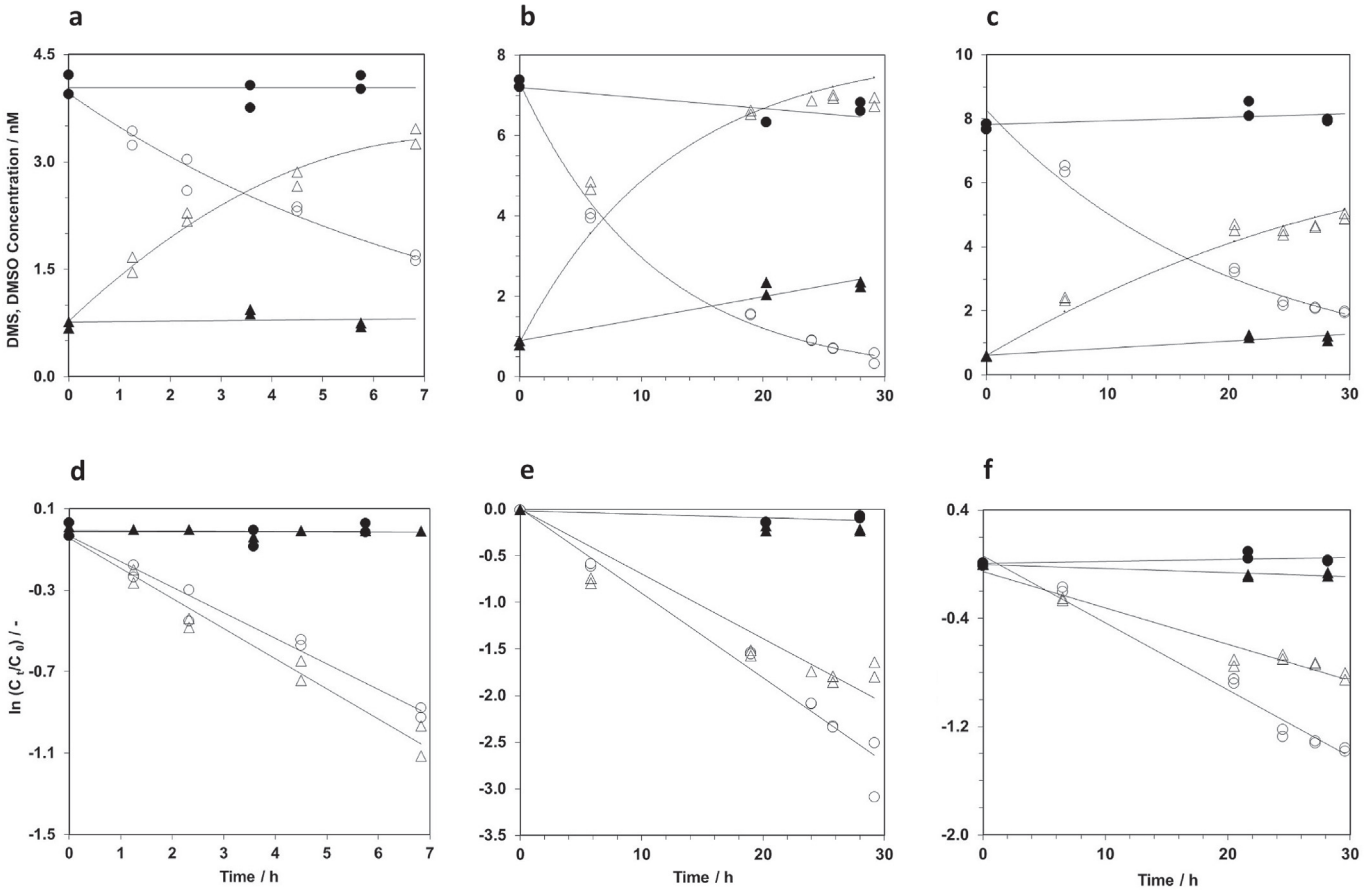

Fig. 2. Time courses of DMS and DMSO concentrations during irradiations No. 6 (Wylam, a), 20 (North Shields, b), and 24 (North Sea, c), and their log-linearised versions (d,e,f). DMS and DMSO concentrations in irradiated samples are shown as open circles and triangles, respectively, and dark controls are shown as the corresponding filled symbols. Solid lines indicate the best fits to the first order rate law (equation (3)). Coefficients of determination for DMS and DMSO were $R^2 = 0.971$ and $R^2 = 0.974$ for irradiation No 6, $R^2 = 0.974$ and $R^2 = 0.922$ for irradiation No 20, and $R^2 = 0.984$ and $R^2 = 0.956$ for irradiation No 24 ($n = 12$).

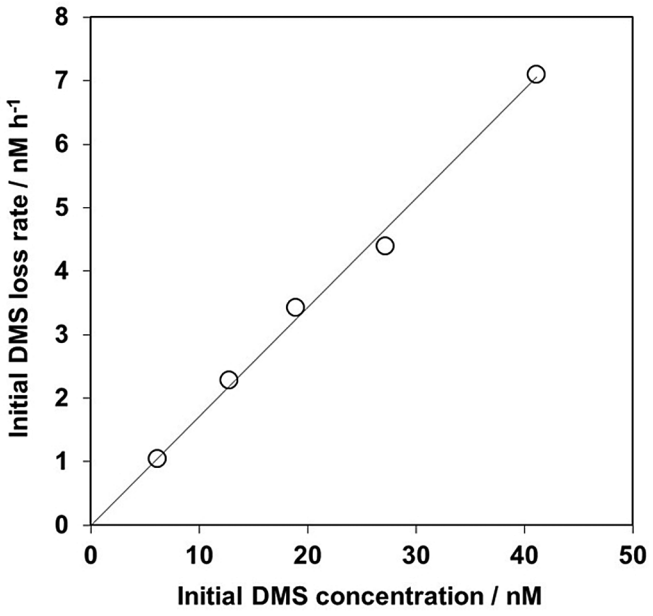

Fig. 3. Initial DMS photo-oxidation rates as a function of initial DMS concentration for a sample collected at the head of the Tyne estuary at Wylam (25 July 2004). The solid line indicates the best fit ($R^2 = 0.995$, $n = 5$).

Table 1), they were still significantly higher than previously reported yields for the northern North Sea (5–37%; Hatton, 2002), the equatorial Pacific (14%; Kieber et al., 1996) and the subpolar South Pacific (33–45%; Toole et al., 2004). Our findings clearly indicate that DMS photo-oxidation by pathways other than photosensitised oxidation by $^1O_2$ (Bouillon and Miller, 2004; Toole et al., 2004) is of only minor importance for the estuarine and coastal waters studied here. By contrast, contributions to DMS photo-oxidation from nitrate related pathways, extrapolated from the nitrate dependence of DMS photo-oxidation rates, were important in the subpolar South Pacific (35%) and NE Pacific (81%) (Bouillon and Miller, 2004; Toole et al., 2004). To date, DMSO yields (33–45%), a proxy for the $^1O_2$ pathway contribution to DMS photo-oxidation (Kieber et al., 1996), and concurrent contributions from nitrate related pathways (35%) have only been reported in Toole et al. (2004), for the subpolar South Pacific. Findings by Toole et al. (2004) imply overall contributions of 68–80% from singlet-oxygen and nitrate related pathways combined, and therefore suggest a contribution of 20–32% from CDOM related pathways other than those involving $^1O_2$ and DMSO formation. In summary, further research is required to resolve the varying contributions of individual DMS removal pathways and their underlying mechanisms.

3.2. Variability of DMS photo-oxidation rates and relationship to CDOM

Pseudo first order DMS photo-oxidation rate constants and

DMSO photoproduction rate constants both varied nearly 10-fold, with highest values (0.345 h^{-1} and 0.283 h^{-1} respectively) near the head of the Tyne estuary and lowest values (0.038 h^{-1} and 0.017 h^{-1} respectively) in the adjacent coastal North Sea (Table 1). We tested for correlations between rate constants on the one hand and salinity, CDOM characteristics (a_{350}, $S_{290\text{-}350}$), and first order rate constants for the absorption coefficient (a_{350}) and CDOM spectral slope ($S_{290\text{-}350}$) photobleaching on the other, to gain an insight into what controls the variability in photochemical DMS conversion. We considered photobleaching rate constants, because we observed significant decreases in a_{350} concurrent with increases in $S_{290\text{-}350}$ in our irradiations, and because photobleaching rate constants may reflect CDOM nature and photoreactivity (Rodríguez-Zúñiga et al., 2008). Average first order rate constants of a_{350} photobleaching and $S_{290\text{-}350}$ increase were 0.016 ± 0.005 h^{-1} and 0.006 ± 0.004 h^{-1}, respectively, consistent with previous work in the study area (Kitidis et al., 2008). Experiments 1 and 22–24 (Table 1) were excluded from this correlation analysis, because CDOM photobleaching data were unavailable. Overall, rate constants for DMS photo-oxidation and DMSO photoproduction both showed the strongest relationships with a_{350} (DMS: r = 0.723, n = 22; DMSO: r = 0.824, n = 15; Table 2). They were both also negatively correlated to salinity (DMS: r = −0.607, n = 22; DMSO: r = −0.559, n = 15; Table 2) reflecting the inverse relationship between salinity and a_{350}, (r = −0.491, n = 22, p = 0.02). The weaker correlations for salinity arise at least in part because salinity is a rather weak index of CDOM variations in the source river waters entering our study estuaries (a_{350} = 16.6 to 71.9 m^{-1}, Table 1). Variability in a_{350} alone explained more than 60% and 70% of the observed variability in the rate constants of DMS photo-oxidation (R^2 = 0.61, n = 26) and DMSO photoproduction (R^2 = 0.73, n = 17) (Fig. 4). We therefore suggest that a_{350} can be a useful predictor of DMS photochemical conversion rates in estuarine and coastal waters that have comparable CDOM levels. Interestingly, the intercepts of the regression lines in Fig. 4 imply some residual photoreactivity in the absence of CDOM (k_{DMS} = 0.9 h^{-1}; k_{DMSO} = 0.5 h^{-1}), which may possibly be related to nitrate. However, for a_{350} below 2 m^{-1}, representative of coastal North Sea waters, observed rate constants for both DMS photo-oxidation and DMSO photoproduction fell significantly below the regression lines (Fig. 4). We therefore contend that the trends depicted in Fig. 4 are likely unrepresentative of waters with CDOM absorption coefficients (a_{350}) significantly lower than those for our study area (1.1–71.9 m^{-1}; Table 1).

A strong correlation between DMS photochemical conversion rate constants and CDOM is consistent with the notion of CDOM photosensitised oxidation by $^1O_2$ because steady-state concentrations of DOM derived triplet states involved in $^1O_2$ formation are proportional to mid UV CDOM absorption coefficients (Zepp et al., 1985). Previous findings that DMS photo-oxidation is dominated by UV-A radiation are also consistent with a role for CDOM because in seawater light absorption in the UV-A range is dominated by DOM chromophores (Toole et al., 2004; Taalba et al., 2013). Even so, the evidence for DMS photo-oxidation − CDOM relationships remains scant. Hatton (2002) did not find any correlation between DMS photo-oxidation rate constants and DOC in the northern North Sea, plausibly due to the limited range of DOC concentrations (60–80 μM C), and by implication CDOM levels, encountered. Irradiation experiments with a dilution series of aged Adriatic Sea water indicated a linear increase in initial DMS photo-oxidation rate with increasing DOC concentrations (8–80 μM C) (Brugger et al., 1998), but did not allow any conclusions regarding the variability of DMS photo-oxidation rates across samples of varying DOM composition. In the north-western Atlantic Ocean DMS photo-oxidation rate constants were highest in shelf waters with elevated CDOM absorption coefficients, but no relationships between DMS photo-oxidation, salinity or CDOM characteristics were reported (Toole et al., 2006). However, a recent study from the Canadian Arctic reported apparent quantum yields of DMS photo-oxidation (AQY_{DMS}) as a function of salinity and CDOM spectral slope from 275 to 295 nm, $S_{275\text{-}295}$ (Taalba et al., 2013). AQY_{DMS} remained approximately constant in samples of estuarine character (S < 25) but increased exponentially towards higher salinity and accompanying lower CDOM. This was attributed primarily to differences in CDOM photoreactivity between terrestrial and marine samples, which were also reflected in $S_{275\text{-}295}$, a proposed proxy of terrestrial CDOM (Taalba et al., 2013).

We interrogated our own data for possible differences in the efficiency of photochemical DMS conversion by examining variations in CDOM normalised rate constants (i.e. k_{DMS} and k_{DMSO} divided by a_{350}) with salinity, a_{350} and $S_{290\text{-}350}$. CDOM normalised rate constants of both DMS photo-oxidation and DMSO photoproduction showed little variation in CDOM-rich samples and a steep increase towards low CDOM coastal waters, best described by a power function. Regression result for DMS photo-oxidation and DMSO production were remarkably similar, again consistent with near 1:1 M conversion of DMS to DMSO (DMS: $k/a_{350} = 0.0405 \times a_{350}^{-0.533}$, R^2 = 0.86, n = 26; DMSO: $k/a_{350} = 0.0293 \times a_{350}^{-0.498}$, R^2 = 0.79, n = 17). Pooling both data sets was therefore justified. Variability in a_{350} explained 81% of the overall variability in CDOM normalised rate constants ($k/a_{350} = 0.0353 \times a_{350}^{-0.515}$, R^2 = 0.81, n = 43; Fig. 5). The relationship of CDOM normalised rate constants with salinity was weaker ($k/a_{350} = 0.0007 \times S + 0.0066$, R^2 = 0.74, n = 43; data not shown), chiefly because salinity does not adequately reflect the variability in a_{350} from terrestrial inputs. CDOM normalised rate constants were not related to $S_{290\text{-}350}$ (R^2 = 0.001, n = 43) because substantial variations in $S_{290\text{-}350}$ (0.0133–0.0153 nm^{-1}; Table 1) at low salinities did not cause discernible changes in photochemical DMS conversion efficiency.

The increase in our CDOM normalised rate constants with decreasing a_{350} is consistent with the notion that marine waters have higher photoreactivity with respect to DMS photo-oxidation than terrestrial waters (Taalba et al., 2013; Galí et al., 2016). The higher photoreactivity of seawater samples may in part be attributed to an increasing contribution from nitrate related DMS photo-oxidation with increasing salinity offshore (Taalba et al., 2013). In the upper Tyne estuary, nitrate concentrations are elevated (40–80 μM) but decline rapidly to < 2 μM in the adjacent North Sea (Ahad et al., 2006), similar to those in Loch Linnhe (0–3 μM; Ross et al., 1993). Even so, given that photochemical DMS conversion in our samples seems to be dominated by CDOM related photo-oxidation by $^1O_2$, (see section 3.1), and that coastal nitrate levels are comparatively low, an increasing contribution from nitrate related pathways alone is an unlikely explanation of an approximately 10-fold increase in CDOM normalised rate constants across

Table 2
Pearson's correlation coefficients for the relationships between first order rate constants of DMS photo-oxidation and DMSO photoproduction, salinity and CDOM characteristics. $k(a_{350})$ and $k(S_{290\text{-}350})$ denote first order rate constants of absorption coefficient photo-bleaching at 350 nm and spectral slope changes, respectively. Experiments 1 and 22–24 (Table 1) were excluded from this correlation analysis, because $k(a_{350})$ and $k(S_{290\text{-}350})$ were not obtained. Significance levels are indicated by asterisks (** 0.01 level; * 0.05 level).

	k_{DMS} (n = 22)	k_{DMSO} (n = 15)
Salinity	−0.607**	−0.559**
a_{350}	0.723**	0.824**
$S_{290\text{-}350}$	−0.356**	−0.711**
$k(a_{350})$	0.510**	0.323**
$k(S_{290\text{-}350})$	0.459**	0.291**

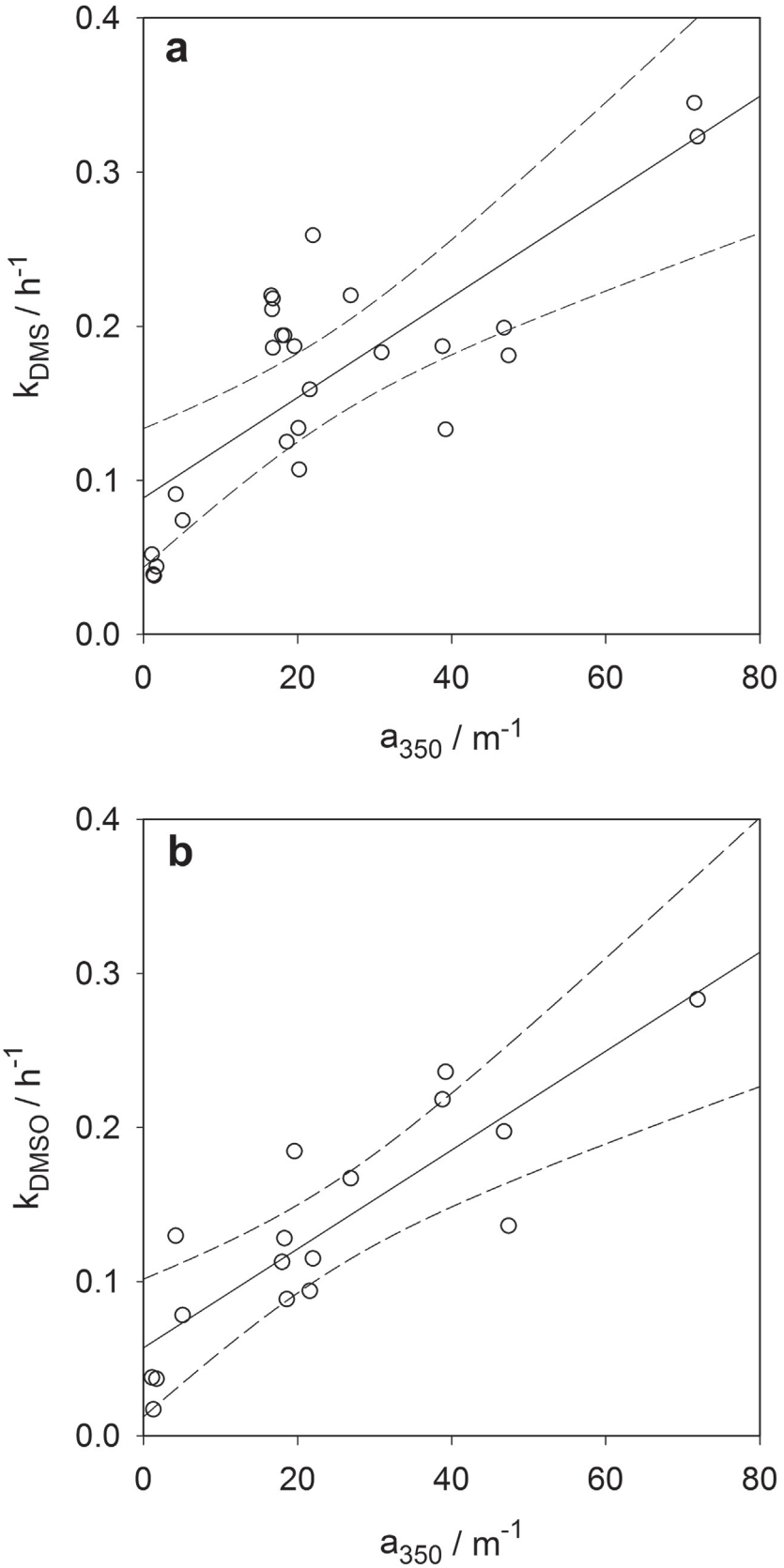

Fig. 4. Relation of pseudo first order rate constants of DMS photo-oxidation (a) and DMSO photoproduction (b) to the CDOM absorption coefficient at 350 nm. The best fit line for DMS photo-oxidation was $k_{DMS} = 0.0033 \times a_{350} + 0.089$ ($R^2 = 0.61$, $n = 26$). The best fit line for DMSO photoproduction was $k_{DMSO} = 0.0032 \times a_{350} + 0.057$ ($R^2 = 0.73$, $n = 17$). Dashed lines indicate 99% confidence intervals.

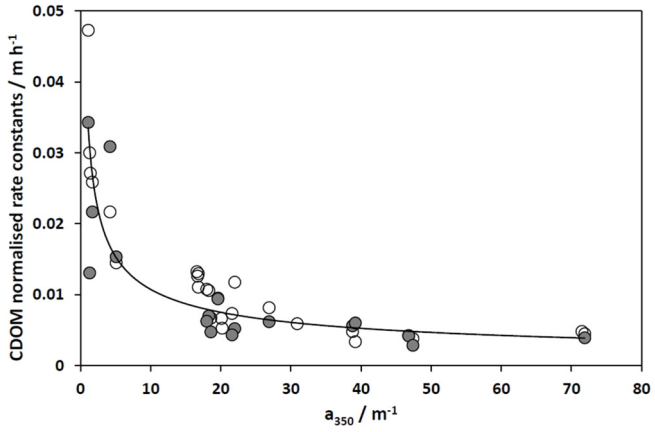

Fig. 5. First order rate constants of DMS photo-oxidation (open circles) and DMSO photoproduction (filled circles), normalised to the CDOM absorption coefficient at 350 nm, a_{350}, as a function of CDOM levels. The solid line indicates the results of a best fit of all data against a power function ($k/a_{350} = 0.0353 \times a_{350}^{-0.515}$; $R^2 = 0.81$, n = 43).

the salinity gradient. Furthermore, strong summer depletion of nitrate in the coastal NE North Sea (nitrate <50 nM; Woodward and Owens, 1990) suggests a low overall contribution from nitrate related DMS photo-oxidation in our study area. More plausibly, compositional differences between terrestrial and marine CDOM were important in defining the variability in CDOM normalised rate constants depicted in Fig. 5. These findings agree with a recent meta-analysis Galí et al. (2016) which concluded that CDOM nature and abundance are the primary controls of DMS photo-oxidation, that any contributions from nitrate related pathways are comparatively low, and that variability in AQY_{DMS} reflects CDOM origin (terrestrial versus marine) and subsequent photobleaching in the upper mixed layer. However, in our study areas the variability in photochemical DMS conversion was overall dominated by changes in CDOM abundance, the lowest rate constants being found in coastal waters with the lowest values of a_{350} (Fig. 4).

3.3. Photochemical DMS turnover and DMSO production

The lower end of our range of DMS photo-oxidation rate constants (0.038–0.345 h^{-1}; Table 1) overlaps with previously reported values from sunlight incubations of coastal seawater in the northern (0.03–0.07 h^{-1}; Hatton, 2002) and south-western North Sea (0.09 h^{-1}; Brimblecombe and Shooter, 1986), the northern Adriatic Sea (0.12 h^{-1}; Brugger et al., 1998) and the north-western Atlantic Ocean (0.03–0.09 h^{-1}; Toole et al., 2006). By contrast, our highest DMS photo-oxidation rate constants are 3–5 fold higher than those previously reported. This may reflect differences in irradiation conditions or in the intrinsic photoreactivity of the seawater samples used. Sunlight incubations on the roof of our Newcastle laboratory simultaneous with our laboratory irradiations enabled us to compare our laboratory results with the ambient sunlight effect (Table 3.). The ratio of DMS photo-oxidation rate constants derived with these two approaches was close to unity for overcast conditions (R(Sun/Sim) = 1.09), but reached a maximum of 1.66 under reduced cloud cover. On average, rate constants determined in sunlight incubations were 1.43 times higher than those determined in the solar simulator. Given that our sunlight irradiations were carried out around midsummer at a latitude similar to or higher than in previous experiments (Brimblecombe and Shooter, 1986; Brugger et al., 1998; Hatton, 2002; Toole et al., 2006), our irradiation conditions most likely do not account for our comparatively high rate constants. We consider it more likely that the high DMS photo-oxidation rate constants we found reflect elevated CDOM levels (Table 1).

To examine the role of varying CDOM levels and thus facilitate further comparison to other work, we grouped our data into upper estuary (S < 20), lower estuary (20 < S < 30), and coastal domains (S > 30) (Table 4). The mean a_{350} of these sample groupings broadly agrees with previous work in the study area (Stubbins et al., 2011). Furthermore, the mean CDOM absorption coefficient for our coastal samples ($a_{350} = 1.4\ m^{-1}$) is similar to the mean a_{350} value of 1.3 m^{-1} for the North Sea, obtained by extrapolation from $a_{442} = 0.348\ m^{-1}$ (Tilstone et al., 2012) using a CDOM spectral slope of 0.014 nm^{-1} (Table 1). Our mean coastal DMS photo-oxidation rate constant, k_{DMS}, was 1.0 d^{-1}, 2-fold and 5-fold lower than our means for the lower and upper estuary, respectively (Table 4). To scale our mean rate constants to the daily mean solar irradiance in our study area in July we multiplied our mean k_{DMS} values by (i) the mean ratio of k_{DMS} from sunlight irradiations to that determined under artificial light (R(Sun/Sim) = 1.43), and (ii) the ratio of daily global clear sky irradiance (317 W m^{-2}) to the average global clear sky irradiance (775 W m^{-2}) from SMARTS2 (Gueymard, 2001) over the duration of our sunlight irradiations. The scaled DMS photo-oxidation rate constants, k'_{DMS} (Table 4), were approximately 2-fold lower than the unscaled values from our laboratory irradiations, but still equal to or exceeding the median daily DMS photo-oxidation rate constants for river-influenced coastal surface waters (0.58 d^{-1}; Galí et al. (2016)).

The most rigorous calculations of photochemical DMS turnover in the water column are based on apparent quantum yields and wavelength resolved underwater irradiance (Toole et al., 2003; Bouillon et al., 2006; Taalba et al., 2013). Because we did not obtain wavelength resolved DMS photo-oxidation rates or underwater irradiance data, we constrained the effects of underwater light attenuation by scaling to mid-UV underwater irradiance at 350 nm. Following Zepp et al. (1987), we estimated mean DMS photo-oxidation rate constants in the water column, k^{int}_{DMS}, from

$$k^{int}_{DMS} = (k'_{DMS} \exp(1 - K_{d,350}\, z))/(K_{d,350}\, z) \quad (5)$$

where z is water column depth and $K_{d,350}$ is the light attenuation coefficient at 350 nm. $K_{d,350}$ was estimated from CDOM absorbance

Table 3
Comparison of simultaneous sunlight and laboratory irradiation experiments of water samples collected at the head of the Tyne estuary (Wylam). Average conditions are given for the sunlight exposure period (10–14:00 UTC). UV irradiance was measured with a broad band UV sensor (UVAB, Delta-T Devices). The pseudo first order rate constants of DMS photo-oxidation, k_{DMS}, were derived from sunlight irradiations on the roof of the Newcastle laboratory. R(Sun/Sim) denotes the ratio of k_{DMS} from sunlight irradiations to the k_{DMS} determined simultaneously on the Newcastle solar simulator. The mean R(Sun/Sim) was 1.43.

No.	Irradiation Date	Conditions	UV/W m^{-2}	a_{350}/m^{-1}	k_{DMS}/h^{-1}	R(Sun/Sim)
1	13/07/2004	Broken clouds	18.5	71.6	0.737 ± 0.060	1.64
2	21/07/2004	Overcast to clear	18.0	16.8	0.250 ± 0.018	1.29
3	23/07/2004	Scattered clouds	22.9	16.8	0.362 ± 0.014	1.66
4	27/07/2004	Broken to scattered clouds	20.1	16.7	0.314 ± 0.022	1.49
5	02/08/2004	Overcast to hazy	11.2	16.6	0.246 ± 0.019	1.09

Table 4
Mean DMS photo-oxidation rate constants from the study area. Water depth was calculated from data in Stubbins et al. (2011). Light attenuation coefficients at 350 nm, $K_{d,350}$, were estimated from CDOM absorbance. k'_{DMS} refers to the DMS photo-oxidation rate constant scaled to mean daily irradiance. k^{int}_{DMS} refers to the mean DMS photo-oxidation rate constant in the water column. See text for details.

Salinity range	Water depth/m	a_{350}/m^{-1}	$K_{d,350}/m^{-1}$	Solar simulator	Scaled	Water column average
				k_{DMS}/d^{-1}	k'_{DMS}/d^{-1}	k^{int}_{DMS}/d^{-1}
Upper estuary (S < 20)	6	29.9	39.9	4.8	2.8	0.012
Lower estuary (20 < S < 30)	10	4.7	6.2	2.0	1.2	0.019
Coastal (S > 30)	20	1.4	1.8	1.0	0.6	0.017

according to Preisendorfer (1976),

$$K_{d,350} = 4\,(a_{350} + a_{w,350}) / 3 \quad (6)$$

where $a_{w,350}$ is the light absorption coefficient of pure water at 350 nm (Buiteveld et al., 1994). Scaling to underwater irradiance appears justified given that water column DMS photo-oxidation was previously found to be dominated by UV-A wavelengths (Toole et al., 2003; Deal et al., 2005; Taalba et al., 2013). Estimating $K_{d,350}$ from CDOM absorbance introduces some additional uncertainty, although previous work by Farmer et al. (1993) in the Orinoco River plume found generally good agreement between $K_{d,350}$ predicted from equation (6) and direct observations. Even so, scattering and absorbance by particulate matter likely contributed significantly to overall light attenuation in our study area (Stubbins et al., 2011). Therefore, our estimates of $K_{d,350}$ in Table 4 should be regarded as lower limits and consequently, our water column averaged DMS photo-oxidation rate constants should be viewed as upper limits.

Our estimates of water column averaged DMS photo-oxidation rate constants, k^{int}_{DMS}, span a rather narrow range: 0.012 to 0.019 d^{-1} (Table 4). In the upper estuary, k^{int}_{DMS} was lowest, plausibly due to a shallow optical depth (i.e. $(K_{d,350})^{-1} < 0.03$ m) caused by high light attenuation. Deeper optical depths in lower estuary (0.2 m) and in coastal waters (0.7 m) counteracted the lower DMS photo-oxidation rate constants, resulting in slightly higher k^{int}_{DMS}. Our water column averaged DMS photo-oxidation rate constants fall towards the low end of a recently compiled range (Taalba et al., 2013), in which the lowest k^{int}_{DMS} were for the Canadian Arctic (0.01–0.03 d^{-1}), Bering Sea (0.02–0.11 d^{-1}) and subarctic NE Pacific (0.03–0.25 d^{-1}) (Deal et al., 2005; Bouillon et al., 2006; Taalba et al., 2013), and highest values were for the subpolar North Atlantic (0.04–2.5 d^{-1}) (Simó and Pedrós-Alió, 1999). For the subpolar North Atlantic, photochemical water column turnover rate constants were determined indirectly from the difference between the net of total DMS loss and its biological consumption, and estimates of air sea gas exchange. They should therefore be regarded as somewhat uncertain. The highest k^{int}_{DMS} values derived from controlled irradiation experiments were for the Ross (0.5–0.71 d^{-1}) and Greenland Seas (0.23–1.05 d^{-1}) (Toole et al., 2004; Galí and Simó, 2010). High turnover rate constants in the Ross Sea were attributed to a combination of high nitrate levels, enhanced CDOM photoreactivity and high daily irradiance during the austral Summer (Toole et al., 2004), while high upper mixed layer-integrated rate constants for the Greenland Sea are due at least in part to shallow, ice melt induced stratification (Galí and Simó, 2010). Given that seawater photoreactivity appears to increase offshore, presumably due to an increasing contribution by nitrate photochemistry and the higher photoreactivity of marine CDOM (Bouillon and Miller, 2004; Toole et al., 2004; Taalba et al., 2013), our low k^{int}_{DMS} can be partly explained by the lower photoreactivity of CDOM-rich, near coastal waters (Fig. 5) and partly by higher light attenuation in our study area ($K_{d,350} > 1.8$ m^{-1}) than was encountered by Toole et al. (2004) in the clear waters of the Ross Sea ($K_d = 0.085$ m^{-1}). Estimates of k^{int}_{DMS} are also sensitive to the choice of water column depth (equation (5)). For our work we chose bathymetric depth (Stubbins et al., 2011) because the water columns in our study area are predominantly well mixed (van Leeuwen et al., 2015). Even so, freshwater induced stratification can lead to upper mixed layer depths of 2–10 m in the lower Tyne estuary and adjacent North Sea (Rodrigues et al., 2007). For illustration, using an upper mixed layer depth of 2–10 m would return k^{int}_{DMS} of 0.03–0.16 d^{-1} for coastal waters (S > 30), in broad agreement with estimates for the Mackenzie Shelf (0.01–0.11 d^{-1}) where mixed layer depths are comparably shallow, at 1–4.5 m (Taalba et al., 2013). In conclusion, our rate constants for DMS water column turnover are broadly comparable with previous work in coastal waters with elevated CDOM levels and high light attenuation, but they are somewhat lower than those for the clearest open ocean waters.

Previous studies reported a variable contribution from DMS photo-oxidation to overall DMS removal of around 6–70% (Kieber et al., 1996; Archer et al., 2002; Toole et al., 2003, 2004; Bouillon et al., 2006; Galí and Simó, 2010, 2015), and indicated that photo-oxidation can typically dominate over losses through biological consumption and air-sea gas exchange during periods of strong stratification with shallow mixed layer depths (Toole et al., 2006; Galí and Simó, 2010). However, a recent meta-analysis of DMS cycling rates suggest that the combined contributions of photochemical and air-sea gas exchange losses generally fall below 20% (Galí and Simó, 2015). Our low water column integrated DMS photo-oxidation rate constants suggest long photochemical turnover times of 86, 53, and 61 days for upper, lower estuarine and coastal waters, respectively. For comparison, we calculated ventilation turnover times based on water depths from Table 4, summer means of DMS concentrations for western European estuaries (3.77 nM) and shelves (8.43 nM), wind speed at 10 m height and seawater temperature, taken from Uher (2006). DMS fluxes were calculated according to Nightingale et al. (2000). Gas transfer velocities were corrected for their Schmidt number (Sc) dependence by multiplying with $(Sc/660)^{-0.5}$, using the parameterisation of Saltzman et al. (1993). Our ventilation turnover times were 2.3, 3.8, and 7.5 days for upper, lower estuary and coastal waters, respectively, i.e. one order of magnitude lower than the photochemical turnover times. In coastal waters, photochemical losses only accounted for about 12% of the loss by air-sea gas exchange. Concurrent rate data for DMS biological consumption are not available for our study area. However, recent work in UK coastal waters indicated summertime biological turnover times of 0.6–2.7 days (Hopkins and Archer, 2014), significantly faster than photo-oxidation. Our comparison thus implies that photochemical removal of DMS is probably of only minor importance in our study area.

4. Summary and conclusions

We found near 1:1 M conversion of DMS to DMSO in irradiations

of estuarine samples (S < 30), consistent with photosensitised DMS photo-oxidation by $^1O_2$. On this basis, we contend that this is the predominant pathway for photochemical DMS removal in our study area. The variability we observed in photo-oxidation rate constants along our river-sea transect is largely attributable to varying CDOM levels, as reflected in a_{350} (Fig. 4). Overall, however, high sea surface DMS photo-oxidation rate constants in areas of highest CDOM abundance were counterbalanced by low mid-UV optical depths, such that mean daily water column photo-oxidation rate constants (k^{int}_{DMS}) showed little variation between riverine, estuarine and coastal areas. However, strong increases in the CDOM-normalised rate constants of DMS photo-oxidation and DMSO production towards low CDOM levels in coastal North Sea waters (Fig. 5) implies that marine waters are more reactive than estuarine waters with respect to DMS photo-oxidation. This higher photoreactivity may be explained by a combination of an increased contribution from nitrate related DMS photo-oxidation and a higher photoreactivity of marine-derived CDOM, as previously suggested (Toole et al., 2004; Taalba et al., 2013). The high photoreactivity of coastal samples (S > 30) is reflected in CDOM normalised DMS photo-oxidation rate constants (mean = 0.034 m h^{-1}; Fig. 5), the lowest DMSO yields (mean = 60%, n = 3; Table 1) and by implication the lowest contribution from the $^1O_2$ pathway to DMS photo-oxidation. Photosensitised oxidation by $^1O_2$ may thus be less effective than other photochemical removal pathways. Progress in defining the complex relationship between CDOM and DMS photo-oxidation will require an improved understanding of these various underlying mechanisms.

Our comparatively long photochemical turnover times (53–86 days, section 3.3) are consistent with low seawater photoreactivity combined with shallow optical depths in the mid UV (<0.03–0.7 m). Assuming our DMS photo-oxidation rate constants to broadly represent other estuarine and near coastal waters, corresponding contributions from photochemical DMS removal to overall losses are likely to be minor albeit still significant. In near coastal waters, photochemical removal likely dominates only in conditions of shallow stratification, low rates of air-sea gas exchange due to low wind speeds and low biological consumption in near surface waters (Toole et al., 2006; Galí and Simó, 2010). We believe that further research in this field should focus on the balance of DMS removal processes during periods of shallow stratification.

Acknowledgements

We would like to thank the crews of RV *Bernicia* and RV *Seol Mara*, and Jonathan Barnes and Vassilis Kitidis for their assistance with seawater sampling. Gordon Henry assisted in setting up the Newcastle solar simulator and with GC-SCD analyses. J. Julian Pillans was supported by a UK Natural Environment Research Council studentship (NER/S/A/2001/06647). We thank two anonymous reviewers for their insightful comments that helped us to improve our manuscript.

References

Ahad, J.M.E., Ganeshram, R.S., Spencer, R.G.M., Uher, G., Upstill-Goddard, R.C., Cowie, G.L., 2006. Evaluating the sources and fate of anthropogenic dissolved inorganic nitrogen (DIN) in two contrasting North Sea estuaries. Sci. Total Environ. 372, 317–333.

Archer, S.D., Gilbert, F.J., Nightingale, P.D., Zubkov, M.V., Taylor, A.H., Smith, G.C., Burkill, P.H., 2002. Transformation of dimethylsulphoniopropionate to dimethyl sulphide during summer in the North Sea with an examination of key processes via a modelling approach. Deep-Sea Res. Part II Top. Stud. Oceanogr. 49, 3067–3101.

Bentley, R., Chasteen, T.G., 2004. Environmental VOSCs––formation and degradation of dimethyl sulfide, methanethiol and related materials. Chemosphere 55, 291.

Bouillon, R.-C., Miller, W.L., Levasseur, M., Scarratt, M., Merzouk, A., Michaud, S., Ziolkowski, L., 2006. The effect of mesoscale iron enrichment on the marine photochemistry of dimethylsulfide in the NE subarctic Pacific. Deep Sea Res. Part II Top. Stud. Oceanogr. 53, 2384–2397.

Bouillon, R.C., Miller, W.L., 2004. Determination of apparent quantum yield spectra of DMS photo-degradation in an in situ iron-induced Northeast Pacific Ocean bloom. Geophys. Res. Lett. 31.

Brimblecombe, P., Shooter, D., 1986. Photo-oxidation of dimethylsulphide in aqueous solution. Mar. Chem. 19, 343–353.

Brugger, A., Slezak, D., Obernosterer, I., Herndl, G.J., 1998. Photolysis of dimethylsulfide in the northern Adriatic Sea: dependence on substrate concentration, irradiance and DOC concentration. Mar. Chem. 59, 321–331.

Buiteveld, H., Hakvoort, J.H.M., Donze, M., 1994. Optical Properties of Pure Water. In: Ocean Optics XII. SPIE, Bergen, Norway, pp. 174–183.

Carslaw, K.S., Boucher, O., Spracklen, D.V., Mann, G.W., Rae, L., J, G., Woodward, S., Kulmala, M., 2010. A review of natural aerosol interactions and feedbacks within the Earth system. Atmos. Chem. Phys. 10, 1701–1737.

Carslaw, K.S., Lee, L.A., Reddington, C.L., Pringle, K.J., Rap, A., Forster, P.M., Mann, G.W., Spracklen, D.V., Woodhouse, M.T., Regayre, L.A., Pierce, J.R., 2013. Large contribution of natural aerosols to uncertainty in indirect forcing. Nature 503, 67–71.

Charlson, R.J., Lovelock, J.E., Andreae, M.O., Warren, S.G., 1987. Oceanic phytoplankton, atmospheric sulphur, cloud albedo and climate. Nature 326, 655–661.

Deal, C.J., Kieber, D.J., Toole, D.A., Stamnes, K., Jiang, S., Uzuka, N., 2005. Dimethylsulfide photolysis rates and apparent quantum yields in Bering Sea seawater. Cont. Shelf Res. 25, 1825–1835.

Del Valle, D.A., Kieber, D.J., Bisgrove, J., Kiene, R.P., 2007a. Light-stimulated production of dissolved DMSO by a particle-associated process in the Ross Sea, Antarctica. Limnol. Oceanogr. 52, 13–13.

Del Valle, D.A., Kieber, D.J., Kiene, R.P., 2007b. Depth-dependent fate of biologically-consumed dimethylsulfide in the Sargasso Sea. Mar. Chem. 103, 197–208.

Farmer, C.T., Moore, C.A., Zika, R.G., Sikorski, R.J., 1993. Effects of low and high Orinoco river flow on the underwater light field of the eastern Caribbean basin. J. Geophys. Res. 98, 2279–2288.

Galí, M., Kieber, D.J., Romera-Castillo, C., Kinsey, J.D., Devred, E., Pérez, G.L., Westby, G.R., Marrasé, C., Babin, M., Levasseur, M., Duarte, C.M., Agustí, S., Simó, R., 2016. CDOM sources and photobleaching control quantum yields for oceanic DMS photolysis. Environ. Sci. Technol. 50, 13361–13370.

Galí, M., Simó, R., 2010. Occurrence and cycling of dimethylated sulfur compounds in the Arctic during summer receding of the ice edge. Mar. Chem. 122, 105–117.

Galí, M., Simó, R., 2015. A meta-analysis of oceanic DMS and DMSP cycling processes: disentangling the summer paradox. Glob. Biogeochem. Cycles 29, 2014GB004940.

Gueymard, C.A., 2001. Parameterized transmittance model for direct beam and circumsolar spectral irradiance. Sol. Energy 71, 325–346.

Hatton, A.D., 2002. Influence of photochemistry on the marine biogeochemical cycle of dimethylsulphide in the northern North Sea. Deep Sea Res. Part II Top. Stud. Oceanogr. 49, 3039–3052.

Hatton, A.D., Malin, G., McEwan, A.G., Liss, P.S., 1994. Determination of dimethyl sulfoxide in aqueous solution by an enzyme-linked method. Anal. Chem. 66, 4093–4096.

Hope, D., Billett, M.F., Milne, R., Brown, T.A.W., 1997. Exports of organic carbon in British rivers. Hydrol. Process. 11, 325–344.

Hopkins, F.E., Archer, S.D., 2014. Consistent increase in dimethyl sulfide (DMS) in response to high CO2in five shipboard bioassays from contrasting NW European waters. Biogeosciences 11, 4925–4940.

Joint Nature Conservation Committee, 2011. Towards an Assessment of the State of UK Peatlands. JNCC report No. 445.

Kieber, D.J., Jiao, J.F., Kiene, R.P., Bates, T.S., 1996. Impact of dimethylsulfide photochemistry on methyl sulfur cycling in the equatorial Pacific Ocean. J. Geophys. Res. 101, 3715–3722.

Kitidis, V., Stubbins, A.P., Uher, G., Upstill Goddard, R.C., Law, C.S., Woodward, E.M.S., 2006. Variability of chromophoric organic matter in surface waters of the Atlantic Ocean. Deep-Sea Res. Part II Top. Stud. Oceanogr. 53, 1666–1684.

Kitidis, V., Uher, G., Woodward, E.M.S., Owens, N.J.P., Upstill-Goddard, R.C., 2008. Photochemical production and consumption of ammonium in a temperate river-sea system. Mar. Chem. 112, 118–127.

Kloster, S., Feichter, J., Maier-Reimer, E., Six, K.D., Stier, P., Wetzel, P., 2006. DMS cycle in the marine ocean-atmosphere system - a global model study. Biogeosciences 3, 29–51.

Lana, A., Bell, T.G., Simó, R., Vallina, S.M., Ballabrera-Poy, J., Kettle, A.J., Dachs, J., Bopp, L., Saltzman, E.S., Stefels, J., Johnson, J.E., Liss, P.S., 2011. An updated climatology of surface dimethlysulfide concentrations and emission fluxes in the global ocean. Glob. Biogeochem. Cycles 25.

Lana, A., Simó, R., Vallina, S.M., Dachs, J., 2012. Potential for a biogenic influence on cloud microphysics over the ocean: a correlation study with satellite-derived data. Atmos. Chem. Phys. 12, 7977–7993.

Land, P.E., Shutler, J.D., Bell, T.G., Yang, M., 2014. Exploiting satellite earth observation to quantify current global oceanic DMS flux and its future climate sensitivity. J. Geophys. Res. Oceans 119, 7725–7740.

Lee, P.A., de Mora, S.J., Levasseur, M., 1999. A review of dimethylsulfoxide in aquatic environments. Atmos.-Ocean 37, 439–456.

Manning, A.J., 2012. TR167 – Enhanced UK Estuaries Database: Explanatory Notes and Metadata. HR Wallingford Report DDY0427-RT002-R02-00.

Nightingale, P.D., Malin, G., Law, C.S., Watson, A.J., Liss, P.S., Liddicoat, M.I., Boutin, J., Upstill-Goddard, R.C., 2000. *In situ* evaluation of air-sea gas exchange parameterizations using novel conservative and volatile tracers. Glob. Biogeochem. Cycles 14, 373–387.

Preisendorfer, R.W., 1976. Properties. Hydrologic Optics. US Department of Commerce, NOAA Environmental Research Laboratory, Washington D. C., pp. 255–259

Quinn, P.K., Bates, T.S., 2011. The case against climate regulation via oceanic phytoplankton sulphur emissions. Nature 480, 51–56.

Rodrigues, P.P.G.W., Barnes, J., Upstill-Goddard, R.C., 2007. Simulating estuarine nitrous oxide production by means of a dynamic model. Mar. Pollut. Bull. 54, 164–172.

Rodríguez-Zúñiga, U.F., Milori, D.M.B.P., Da Silva, W.T.L., Martin-Neto, L., Oliveira, L.C., Rocha, J.C., 2008. Changes in optical properties caused by UV-irradiation of aquatic humic substances from the Amazon River basin: seasonal variability evaluation. Environ. Sci. Technol. 42, 1948–1953.

Ross, A.H., Gurney, W.S.C., Health, M.R., Hay, S.J., Henderson, E.W., 1993. A strategic simulation model of a fjord ecosystem. Limnol. Oceanogr. 38, 128–153.

Saltzman, E.S., King, D.B., Holmen, K., Leck, C., 1993. Experimental determination of the diffusion coefficient of dimethylsulfide in water. J. Geophys. Res. 98, 16,481–416,486.

Simó, R., 2001. Production of atmospheric sulfur by oceanic plankton: biogeochemical, ecological and evolutionary links. Trends Ecol. Evol. 16, 287–294.

Simo, R., Dachs, J., 2002. Global ocean emission of dimethylsulfide predicted from biogeophysical data. Glob. Biogeochem. Cycles 16 art. no.-1078.

Simó, R., Pedrós-Alió, C., 1999. Short-term variability in the open ocean cycle of dimethylsulfide. Glob. Biogeochem. Cycles 13, 1173–1181.

Spencer, R.G.M., Ahad, J.M.E., Baker, A., Cowie, G.L., Ganeshram, R., Upstill-Goddard, R.C., Uher, G., 2007a. The estuarine mixing behaviour of peatland derived dissolved organic carbon and its relationship to chromophoric dissolved organic matter in two North Sea estuaries (UK). Estuar. Coast. Shelf Sci. 74, 131–144.

Spencer, R.G.M., Baker, A., Ahad, J.M.E., Cowie, G.L., Ganeshram, R., Upstill-Goddard, R.C., Uher, G., 2007b. Discriminatory classification of natural and anthropogenic waters in two U.K. estuaries. Sci. Total Environ. 373, 305–323.

Stedmon, C.A., Nelson, N.B., 2014. The optical properties of DOM in the ocean. In: Hansell, D.A., Carlson, C.A. (Eds.), Biogeochemistry of Marine Dissolved Organic Matter, second ed. Academic Press, Amsterdam, p. 712.

Stern, D.I., 2006. Reversal of the trend in global anthropogenic sulfur emissions. Glob. Environ. Change 16, 207–220.

Stubbins, A., Law, C.S., Uher, G., Upstill-Goddard, R.C., 2011. Carbon monoxide apparent quantum yields and photoproduction in the Tyne estuary. Biogeosciences 8, 703–713.

Sysak, P.K., Foote, C.S., Ching, T.-Y., 1977. Chemistry of singlet oxygen-XXV. Photooxygenation of methionine. Photochem. Photobiol. 26, 19–27.

Taalba, A., Xie, H., Scarratt, M.G., Bélanger, S., Levasseur, M., 2013. Photooxidation of dimethylsulfide (DMS) in the Canadian arctic. Biogeosciences 10, 6793–6806.

Tilstone, G.H., Peters, S.W.M., van der Woerd, H.J., Eleveld, M.A., Ruddick, K., Schönfeld, W., Krasemann, H., Martinez-Vicente, V., Blondeau-Patissier, D., Röttgers, R., Sørensen, K., Jørgensen, P.V., Shutler, J.D., 2012. Variability in specific-absorption properties and their use in a semi-analytical ocean colour algorithm for MERIS in North Sea and Western English Channel Coastal Waters. Remote Sens. Environ. 118, 320–338.

Toole, D.A., Kieber, D.J., Kiene, R.P., Siegel, D.A., Nelson, N.B., 2003. Photolysis and the dimethylsulfide (DMS) summer paradox in the Sargasso Sea. Limnol. Oceanogr. 48, 1088–1100.

Toole, D.A., Kieber, D.J., Kiene, R.P., White, E.M., Bisgrove, J., del Valle, D.A., Slezak, D., 2004. High dimethylsulfide photolysis rates in nitrate-rich Antarctic waters. Geophys. Res. Lett. 31.

Toole, D.A., Slezak, D., Kiene, R.P., Kieber, D.J., Siegel, D.A., 2006. Effects of solar radiation on dimethylsulfide cycling in the western Atlantic Ocean. Deep-Sea Res. Part I Oceanogr. Res. Pap. 53, 136–153.

Tyssebotn, I.M.B., Kinsey, J.D., Kieber, D.J., Kiene, R.P., Rellinger, A.N., Motard-Côté, J., 2017. Concentrations, biological uptake, and respiration of dissolved acrylate and dimethylsulfoxide in the northern Gulf of Mexico. Limnol. Oceanogr. 62, 1198–1218.

Uher, G., 2006. Distribution and air-sea exchange of reduced sulphur gases in European coastal waters. Estuar. Coast. Shelf Sci. 70, 338–360.

Uher, G., Andreae, M.O., 1997. Photochemical production of carbonyl sulfide in North Sea water: a process study. Limnol. Oceanogr. 42, 432–442.

Uher, G., Hughes, C., Henry, G., Upstill-Goddard, R.C., 2001. Non-conservative mixing behavior of colored dissolved organic matter in a humic-rich, turbid estuary. Geophys. Res. Lett. 28, 3309–3312.

van Leeuwen, S., Tett, P., Mills, D., van der Molen, J., 2015. Stratified and nonstratified areas in the North Sea: long-term variability and biological and policy implications. J. Geophys. Res. Oceans 120, 4670–4686.

Vila-Costa, M., Kiene, R.P., Simo, R., 2008. Seasonal variability of the dynamics of dimethylated sulfur compounds in a coastal northwest Mediterranean site. Limnol. Oceanogr. 53, 198–211.

Woodhouse, M.T., Mann, G.W., Carslaw, K.S., Boucher, O., 2013. Sensitivity of cloud condensation nuclei to regional changes in dimethyl-sulphide emissions. Atmos. Chem. Phys. 13, 2723–2733.

Woodward, E.M.S., Owens, N.J.P., 1990. Nutrient depletion studies in offshore North Sea areas. Neth. J. Sea Res. 25, 57–63.

Zepp, R.G., Hoigné, J., Bader, H., 1987. Nitrate-induced photooxidation of trace organic chemicals in water. Environ. Sci. Technol. 21, 443–450.

Zepp, R.G., Schlotzhauer, P.F., Sink, R.M., 1985. Photosensitized transformations involving electronic energy transfer in natural waters: role of humic substances. Environ. Sci. Technol. 19, 74–81.